ADVANCES IN ATMOSPHERIC SCIENCES, VOL. 27, NO. 2, 2010, 230–242

Direct Climatic Effect of Dust Aerosol in the NCAR Community Atmosphere Model Version 3 (CAM3)

YUE Xu*[1,2,3] (乐 旭), WANG Huijun[1,2] (王会军), LIAO Hong[4,1] (廖 宏), and FAN Ke[2] (范 可)

[1] *Climate Change Research Center, Chinese Academy of Sciences, Beijing* 100029

[2] *Nansen-Zhu International Research Center (NZC), Institute of Atmospheric Physics, Chinese Academy of Sciences, Beijing* 100029

[3] *Graduate University of the Chinese Academy of Sciences, Beijing* 100049

[4] *State Key Laboratory of Atmospheric Boundary Layer Physics and Atmospheric Chemistry, Institute of Atmospheric Physics, Chinese Academy of Sciences, Beijing* 100029

(Received 25 December 2008, revised 28 June 2009)

ABSTRACT

Direct climate responses to dust shortwave and longwave radiative forcing (RF) are studied using the NCAR Community Atmosphere Model Version 3 (CAM3). The simulated RF at the top of the atmosphere (TOA) is -0.45 W m^{-2} in the solar spectrum and $+0.09$ W m^{-2} in the thermal spectrum on a global average. The magnitude of surface RF is larger than the TOA forcing, with global mean shortwave forcing of -1.76 W m^{-2} and longwave forcing of $+0.31$ W m^{-2}. As a result, dust aerosol causes the absorption of 1.1 W m^{-2} in the atmosphere. The RF of dust aerosol is predicted to lead to a surface cooling of 0.5 K over the Sahara Desert and Arabian Peninsula. In the meantime, the upper troposphere is predicted to become warmer because of the absorption by dust. These changes in temperature lead to a more stable atmosphere, which results in increases in surface humidity. The upward sensible and latent heat fluxes at the surface are reduced, largely balancing the surface energy loss caused by the backscattering and absorption of dust aerosol. Precipitation is predicted to decrease moderately on a global scale.

Key words: dust aerosol, radiative forcing, direct radiative effect, general circulation model

Citation: Yue, X., H. J. Wang, H. Liao, and K. Fan, 2010: Direct climatic effect of dust aerosol in the NCAR Community Atmosphere Model Version 3 (CAM3). *Adv. Atmos. Sci.*, **27**(2), 230–242, doi: 10.1007/s00376-009-8170-z.

1. Introduction

As one of the major aerosol species in the troposphere, mineral dust plays an important role in the climate system. Every year, about 1000 to 3000 trillion grams (Tg) of dust mass are entrained into the atmosphere from arid and semiarid areas (Penner et al., 2001). The dust storms influence air quality, reduce visibility, and pose risks to human health. In addition, dust aerosol can alter the earth radiation budget directly by scattering and absorption (Sokolik and Toon, 1996; Shi et al., 2005) or indirectly by influencing the formation and properties of clouds (Sassen, 2002). These environmental and climatic influences make the study of dust aerosol one of the most important topics at this time.

Unlike sulfate aerosol which only scatters solar radiation, dust aerosol influences radiative balance in both the shortwave and longwave spectra. Dust absorbs and scatters both solar and thermal radiation, and meanwhile emits thermal radiation. At the surface, radiative forcing (RF, solar plus infrared) is negative during daytime because of the loss of sunlight by the absorption and back-scattering of dust. However, RF becomes positive during nighttime as a result of the continuous longwave heating by the emission of

*Corresponding author: YUE Xu, yuexu@mail.iap.ac.cn

dust (Cautenet et al., 1991; Claquin et al., 1998). At the top of the atmosphere (TOA), the cooling by the scattering of solar flux is greatly offset by the warming caused by the absorption of solar and thermal radiation, leading to a weak perturbation to net radiation as compared with that at the surface (Miller and Tegen, 1998; Shi et al., 2008).

General circulation models (GCM) coupled with the dust cycle are widely used in the study of the climatic effects of dust (e.g., Miller and Tegen, 1998; Woodward, 2001; Liao et al., 2004). Miller and Tegen (1998) utilized the Goddard Institute for Space Studies (GISS) model to simulate climatic responses to dust aerosol. They found that the radiative effect of dust aerosol is to redistribute heating from the surface to within the dust layer. Consequently, the general circulation shows corresponding adjustment both regionally and globally. Perlwitz et al. (2001) further revealed that the interaction between the dust cycle and the atmosphere reduces dust emission and dust loading on a global scale. These findings improved the understanding of the role of dust in the whole climate system.

The simulated climatic impacts of dust aerosol are highly uncertain. Generally, the RF by dust aerosol is sensitive to the imaginary part of the refractive index (k), particle size distribution, the presence of clouds, the vertical profile of dust, the composition of particles, and so on (Tegen and Lacis, 1996; Liao and Seinfeld, 1998; Claquin et al., 1998; Sokolik and Toon, 1999). The current level of knowledge about the direct radiative effect (DRE) of mineral dust is low as compared to that of other atmospheric aerosols (Penner et al., 2001); more studies on dust DRE are needed to better quantify the climatic effects of dust.

In this study, the DRE of dust aerosol is studied with the NCAR Community Atmosphere Model Version 3 (CAM3, Collins et al., 2004). With the default optical properties, dust distribution, and parameterizations in dynamical processes in CAM3, how does the climate respond to the dust aerosol radiative effect? In addition, we compare results from this work with those obtained in previous studies to see some common features. In the next section, dust simulation and the radiative transfer scheme will be briefly described. Section 3 presents the dust RF and the corresponding responses in meteorological fields. In the last section, the findings of this study are summarized and discussed.

2. Model description and experiments

2.1 *Dust simulation*

CAM Version 3 (CAM3) is an atmospheric GCM that includes the Community Land Model (CLM3), an optional slab ocean model, and a thermodynamic sea ice model. The dynamics and physics in CAM3 have been updated substantially as compared to the implementations in previous versions (Collins et al., 2004). Of the three kinds of horizontal resolutions available for CAM3, the T42 resolution (about $2.8^\circ \times 2.8^\circ$) option is used in our simulation. The model has 26 vertical layers, the top of which is located at 3.5 hPa.

There are four size bins of dust spanning diameters from 0.01 to 10 μm. The dust climatology is produced offline using an aerosol assimilation system (Collins et al., 2001) integrated for present-day conditions. The system consists of the Model for Atmospheric Chemistry and Transport (MATCH) (Rasch et al., 1997) and an assimilation of satellite retrieval of aerosol optical depth. The MATCH is driven by the National Centers for Environmental Prediction (NCEP) meteorological reanalysis data with a horizontal resolution of $1.875^\circ \times 1.875^\circ$. Dust mobilization is mainly determined by the wind friction speed and surface and geographic conditions, such as fractions of land covered by lakes, wetland, snow, and vegetation. Dry deposition processes consider both gravitational settling and turbulent mix-out. Wet deposition includes nucleation scavenging and size-resolved washout in both stratiform and convective clouds (Zender et al., 2003).

2.2 *Radiative transfer scheme*

In the shortwave radiation calculation, the model uses a δ-Eddington approximation with 18 spectral intervals spanning the solar spectrum from 0.12 to 5.0 μm (Collins et al., 2004). The optical parameters for dust, including the specific extinction coefficient (SEC), single scattering albedo (SSA), and asymmetry parameter (AP) are derived from Mie calculations for each size bin (Zender et al., 2003). These parameters are calculated offline and kept constant in the simulations.

With the prescribed K_e, the dust optical thickness (DOT) is calculated as follows (Ginoux et al., 2001):

$$\tau_{i,j}(\lambda) = \sum_{n=1}^{4} K_\mathrm{e}(\lambda)_n M_{i,j,n}\,, \tag{1}$$

where n denotes the four dust bins in the CAM3, and $M_{i,j,n}$ is the dust burden of the nth bin over the grid cell (i, j).

The original longwave radiative scheme of the CAM3 does not consider the longwave radiative effect of dust. Because of the importance of the dust thermal effect (Carlson and Benjamin, 1980; Reddy et al., 2005b; Christopher and Jones, 2007; Huang et al., 2009), we employ an exponential transmission approximation for dust aerosol (Carlson and Benjamin, 1980):

$$\mathrm{T}_\lambda = \exp\left[-D\tau_\lambda\right] \quad , \tag{2}$$

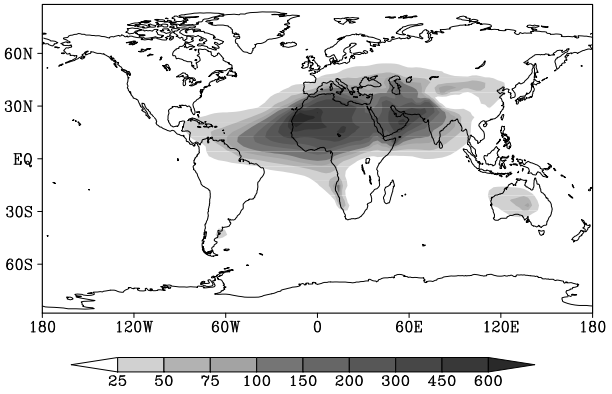

Fig. 1. Simulated annual mean dust column burden in CAM3. Units: mg m^{-2}.

where D is a diffusivity factor set to 1.66, and τ_λ is the total dust optical depth at a specific thermal spectrum λ. Since the spectral intervals in the thermal domain are much larger than those in solar region, each longwave band is divided into small subintervals whose extinction coefficients are then weighted by the spectral intensity denoted as Planck function $B(T, \nu)$. As a result, the SEC K_e over the whole wave band λ could be calculated by (Zhang and Modest, 2002) as

$$K_e(\lambda) = \frac{\sum_i k_i B(T, \nu_i) \Delta\nu}{\sum_i B(T, \nu_i) \Delta\nu} \quad , \tag{3}$$

where k_i and ν_i are the SEC and the medium wavenumber at subinterval i, respectively. Based on the K_e at the thermal wavelength band calculated by Eq. (3), the DOT at the infrared spectrum can be calculated with Eq. (1). For example, the global mean DOT at 10 μm in the CAM3 is 0.005, which is about 16% of that at the visible band. This result is close to the estimation of the 10% in Cautenet et al. (1991) and the 20% in Markowicz et al. (2003).

After obtaining the DOT at infrared bands, we calculate the dust transmissivity with Eq. (2). The atmospheric transmissivity is then multiplied by the dust transmissivity to represent the disturbed air transmission. Scattering of longwave radiation by mineral dust aerosol is neglected, though it may lead to an underestimation of the longwave RF of up to 50% at the TOA and up to 15% at the surface in cloudy conditions (Dufresne et al., 2002).

2.3 *Climate simulation*

The CAM3 calculates the RF of the dust aerosol at all the model layers. The RF is obtained by a "double radiation call" method as described in Woodward (2001) in the CAM3. This method calls the radiation scheme twice at each radiative time step. Dust effects are considered only in the first call, in which the simulated radiative fields are exported rather than fed back into the GCM. In the second call, the model is run normally without dust effects so that the GCM climate is not disturbed. In this way, the climatology of GCM is not affected by dust aerosol while the RF of dust is obtained by the difference in the radiative fluxes of the two calls. We run the CAM3 for 16 months, the first four of which is the spin-up period of the integration. The RF of dust aerosol at each month is obtained.

Two climate simulations are conducted to evaluate the direct climatic effect of dust; the model is run with (denoted as "FED") and without (denoted as "CTRL") dust radiative effects in the radiative transfer scheme of the GCM, respectively. Each experiment is run for 15 years and the meteorological parameters averaged over the last 10 years represent the climatological state of the case. The differences in meteorological fields between these two runs (FED-CTRL) are considered as the direct climatic effect of dust aerosol. The student t-test is used to show the statistical significance of the model results, and only the differences that exceed the 95% confidence level are discussed. The four boreal seasons from spring to winter are denoted by MAM (March–May), JJA (June–August), SON (September–November), and DJF (December–February).

3. Direct climatic effect of dust aerosol

3.1 *Dust concentrations*

Figure 1 shows the dust column density utilized in the CAM3. As expected, the Sahara Desert has the highest concentrations of mineral dust aerosol. High dust concentrations are also found over the Arabian Peninsula. A significant fraction of dust mass is predicted in the Northern Hemisphere (NH); the largest sources of dust in the Southern Hemisphere (SH) are the deserts in Australia. Dust concentrations in central Asia are underestimated. Many studies have shown that the Taklimakan Desert in central Asia and the Gobi Desert in western China emit a great amount of soil mass into the atmosphere, especially in the boreal spring (Wang et al., 2000; Liu et al., 2004; Xie and Xia, 2008). Wu et al. (2005) even obtained a dust burden of about 5000 mg m^{-2} over the Taklimakan Desert. As compared to the site-based observations, the CAM3 underestimates dust concentrations over the Asian sources by about 40%, probably caused by the biased sampling of the complex terrain over those regions (Zender et al., 2003). Except for this bias, the simulated dust distribution is reasonable compared with observations (Prospero et al., 2002) and the simulated global dust burden of 15.6 Tg

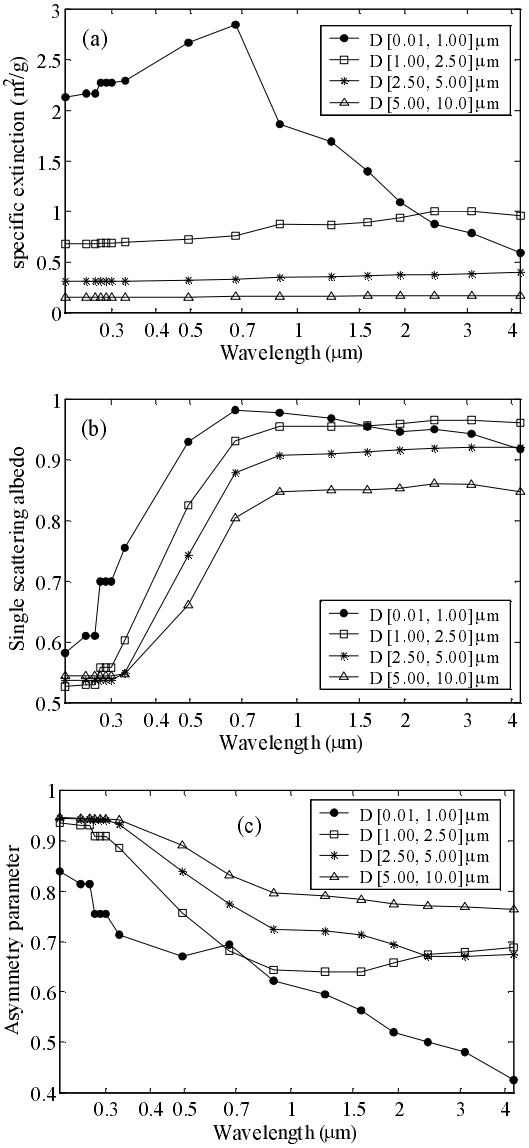

Fig. 2. Optical parameters of dust aerosol used in CAM3. (a) Specific extinction coefficient; (b) single scattering albedo; (c) asymmetry parameter. The D in the legend means "Diameter".

is within the range of 12.1–35.9 Tg obtained by other simulations (e.g., Tegen and Lacis, 1996; Ginoux et al., 2001; Liao et al., 2004; Reddy et al., 2005a; Yue et al., 2009)

3.2 *Dust optical properties*

Figure 2 shows the optical parameters of SEC, SSA, and AP used in the CAM3. The smallest particles have the largest SEC and SSA but the smallest AP for most of the solar wavelength bands, indicating that small particles are efficient in back-scattering of solar radiation. On the contrary, the largest particles have the smallest SSA and are hence more absorptive. However, SEC of large particles is small, constraining the total extinction effect of these particles. As a result, small particles play more important roles in perturbing solar radiation (Yoshioka et al., 2007).

Figure 3 shows the predicted seasonal variation of DOT at 0.67 μm in the CAM3. The largest optical depths exist in boreal summer, with the maximum values located over the Sahara Desert and Arabian Peninsula. The values of DOT in MAM are close to those in JJA in the CAM3. However, the springtime dust activities in central Asia and western China are underestimated as mentioned above. In boreal autumn and winter, dust mobilization over arid and semi-arid sources becomes inactive and the global mean DOT drops to 0.019. The dust sources in Australia show opposite seasonal variation; DOTs in this region are the highest in boreal winter and the lowest in boreal summer. The annual and global mean DOT at 0.67 μm in the CAM3 is 0.029, which is consistent with the value of 0.030 $\pm$ 0.004 estimated in Zender et al. (2003) and the value of 0.029 in Tegen et al. (1997).

Based on the calculated DOT and the prescribed SSA for each dust bins, the annual mean SSA of dust at 0.67 μm is obtained and shown in Fig. 4. SSA values are low over the dust source regions. The minimum value over the Sahara Desert is about 0.94, which is consistent with the observations (e.g., Kaufman et al., 2001; Haywood et al., 2003).

3.3 *The RF of dust aerosol*

The shortwave and longwave RFs of dust aerosol are shown in Fig. 5. The largest forcing values are located over or near dust sources, especially over the Sahara Desert. On a global mean basis, the shortwave forcings at both the TOA and surface are negative, caused by the back-scattering of sunlight by dust particles. However, the magnitude of cooling at the TOA is smaller than that at the surface, because an additional fraction of solar energy is absorbed by dust before solar radiation reaches the surface (Shi et al., 2008). The longwave forcings at both the TOA and surface are positive, which results from the absorption and emission of longwave radiation by dust aerosol (Markowicz et al., 2003).

The simulated global mean dust RFs in the CAM3 are compared with values from other studies in Table 1. All the studies obtained positive thermal RFs, with an average value of +0.19 W m^{-2} at the TOA and of +0.44 W m^{-2} at the surface. The longwave forcings in the CAM3 are +0.09 W m^{-2} at the TOA and +0.31 W m^{-2} at the surface, which are slightly smaller than the averaged values based on previous estimates. The TOA forcings simulated in previous studies were generally negative, except for two cases, the "0.9×ω"

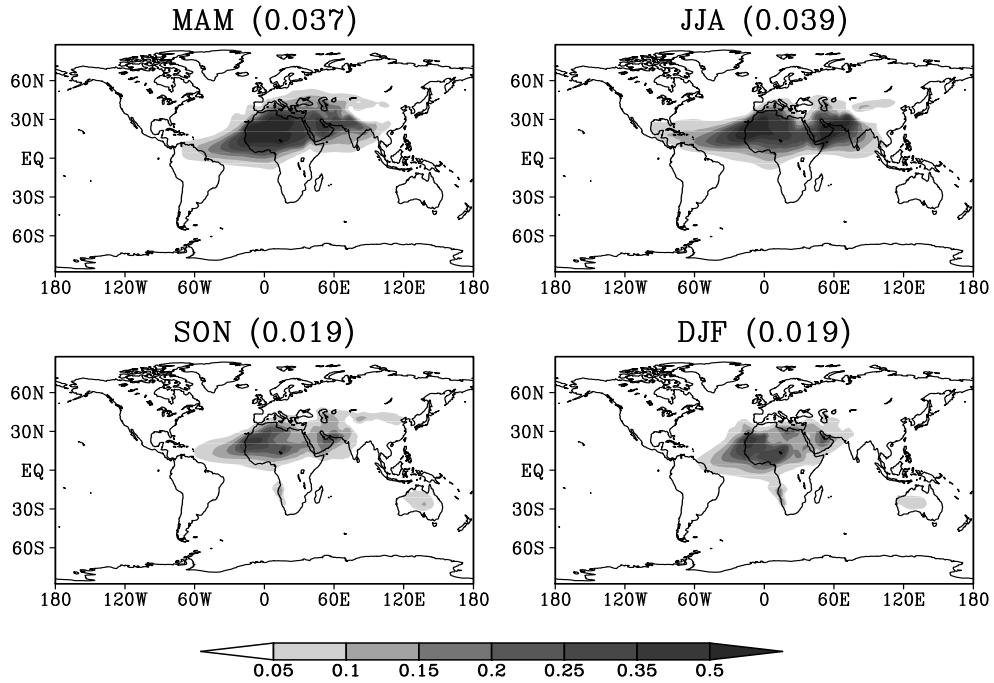

Fig. 3. Seasonal variation of the dust optical depth at 0.67 μm in CAM3. (a) Boreal spring (MAM, March–April–May); (b) boreal summer (JJA, June–July–August); (c) boreal autumn (SON, September–October–November); (d) boreal winter (DJF, December–January–February). The global averages are denoted in the parentheses.

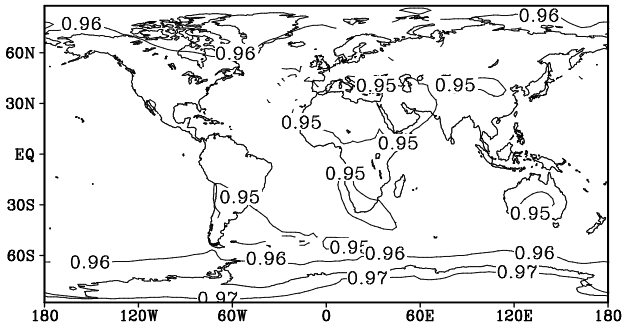

Fig. 4. Simulated distribution of the annual mean single scattering albedo in CAM3.

case in Miller et al. (2004a) and the "Dust-Like" case in Tanaka et al. (2007). Dust particles were more absorptive in these two studies because the SSA was lower or the imaginary part of the refractive index was higher. The average shortwave RF based on previous studies is -0.33 W m^{-2} at the TOA and -1.60 W m^{-2} at the surface, while the values are -0.45 W m^{-2} at the TOA and -1.76 W m^{-2} at the surface in the CAM3.

The above comparison shows that the simulated RF of dust aerosol in the CAM3 is reasonable. The dust-induced change in net radiative fluxes is -0.36 W m^{-2} at the TOA and -1.45 W m^{-2} at the surface; hence 1.1 W m^{-2} (TOA-surface) of energy is absorbed by dust particles in the atmosphere. This result is quite different from that for sulfate aerosol, which only scatters shortwave radiation and leads to a comparatively negative forcing at both the TOA and the surface (Shi et al., 2008). Forster et al. (2007) estimated a sulfate direct RF of -0.41 W m^{-2} based on a number of modeling studies. The TOA RF of dust estimated in our study is comparable to the forcing by sulfate at the TOA. However, the RF of dust is stronger than that of sulfate at the surface.

Dust RF is stronger regionally. As shown in Fig. 5, the strongest shortwave RF at the surface can reach -37.0 W m^{-2}, and the maximum surface-layer longwave RF is 13.2 W m^{-2}. These changes account for 15%–40% of the local total radiative fluxes, indicating the large impacts of dust aerosol.

The seasonal variation of the simulated dust RF is shown in Table 2. Generally, the RF values in MAM and JJA are larger than those in SON and DJF, as a result of the higher dust burdens in MAM and JJA. On the regional scale, the dust RF shows largest response in JJA, when sunlight perpendicularly irradiates the subtropical belt of dust sources. As a result, the local RFs become the largest in this season.

The RF shows the direct impact of dust aerosol on the atmospheric circulation, which has been demonstrated by observations. Ackerman and Chung (1992) used the observations from the Earth Radiation Bud-

Table 1. Annual and global mean dust RF from different models. Units: W m^{-2}.

References	TOA			Surface		
	shortwave	longwave	Net	shotwave	longwave	Net
Miller and Tegen (1998)			−0.07			−2.08
Jacobson (2001)	−0.20	+0.07	−0.14			−0.85
Myhre and Stordal (2001)	−0.02	+0.41	+0.39			
Perlwitz et al. (2001)	−0.50	+0.10	−0.40	−2.10	+0.40	−1.70
Woodward (2001)	−0.16	+0.23	+0.07	−1.22	+0.40	−0.82
Liao et al. (2004)	−0.21	+0.31	+0.10	−1.06	+0.53	−0.53
Miller et al. (2004a)($0.9\times\omega$)	+0.61	+0.15	+0.76	−2.65	+0.18	−2.47
Miller et al. (2004a)	−0.33	+0.15	−0.18	−1.82	+0.18	−1.64
Miller et al. (2004a) ($1.1\times\omega$)	−0.96	+0.14	−0.82	−1.24	+0.17	−1.07
Reddy et al. (2005b)	−0.28	+0.14	−0.14			
Yoshioka et al. (2007)	−0.92	+0.32	−0.60	−1.59	+1.13	−0.46
Shell and Somerville (2007) (ω=0.97)	−0.73	+0.23	−0.49	−1.34	+0.37	−0.97
Shell and Somerville (2007) (ω=0.85)	−0.31	+0.23	−0.07	−2.70	+0.37	−2.33
Tanaka et al. (2007) (ADEC-1)	−0.68	+0.16	−0.52	−0.84	+0.57	−0.27
Tanaka et al. (2007) (ADEC-2)	−0.38	+0.16	−0.22	−1.22	+0.57	−0.65
Tanaka et al. (2007) (OPAC-MD)	−0.17	+0.16	−0.01	−1.49	+0.57	−0.92
Tanaka et al. (2007) (Dust-Like)	+0.03	+0.08	+0.11	−1.54	+0.29	−1.25
Average of above	−0.33	+0.19	−0.13	−1.60	+0.44	−1.20
This study	−0.45	+0.09	−0.36	−1.76	+0.31	−1.45

get Experiment (ERBE) to estimate the RF of dust aerosol. In their estimation, the presence of dust causes between −40 to −90 W m^{-2} of shortwave RF at the TOA around the coast of North Africa. In contrast, dust events are found to increase the net longwave radiation at the TOA by 5–20 W m^{-2} over the oceans and by up to 50 W m^{-2} over the deserts. Haywood et al. (2003) observed a local instantaneous shortwave RF of up to –129 W m^{-2} off the coast of West Africa by aircraft-based measurements. These findings are higher than the annual mean RF values obtained in this work, indicating dust aerosol can have strong radiative impacts during dust events.

We can further examine dust RF during dust events. We use the *in situ* dust event records and aerosol optical depth (AOD) data from the Total Ozone Mapping Spectrometer (TOMS, Torres et al., 2002) to quantify the perturbations of radiative fluxes during dust storms. The ground-based observations are the historical dust event records at 753 stations in China from 1954 to 2007 (Zhou et al., 2002). Based on this dataset, we select the most severe dust event on 12 April 1979 (Zhou and Zhang, 2003); 79 stations over the Loess Plateau reported a "dust storm case" on this day, as shown in Fig. 6a. The TOMS AOD on the same day shows high values over northern China (Fig. 6c). Relative to 9 April 1979, an ordinary weather day has "dust storm case" indications at only 9 stations (Fig. 6b), and the differences in radiative fluxes between 9 and 12 April 1979 assess the RF of dust aerosol.

The daily radiation fields are taken from the European Center for Medium range Weather Forecasting (ECMWF) 40 Years Re-Analysis (ERA-40) data. The dust-induced changes in radiative fluxes are shown in Fig. 7. Both shortwave and longwave radiation show large perturbations to the east of the observed dust events (Figs. 6a, 6c). Such misalignment is caused by the time difference between satellite retrieval and observation at the stations. The pattern of the observed changes in radiative fluxes is similar to that of the simulated dust RFs in the CAM3 (Fig. 5). At both the TOA and the surface, the solar RFs are negative and the thermal RFs are positive. The shortwave

Table 2. Seasonal variation of the global mean dust RF. If the value is positive (negative), the corresponding regional maximum (minimum) is denoted in parentheses. Units: W m^{-2}.

		MAM	JJA	SON	DJF
TOA:	shortwave	−0.60 (−17.0)	−0.49 (−21.9)	−0.34 (−11.4)	−0.38 (−11.6)
	longwave	0.13 (3.4)	0.13 (6.3)	0.05 (1.5)	0.04 (0.8)
Surface:	shortwave	−2.32 (−43.2)	−2.35 (−65.9)	−1.19 (−25.9)	−1.17 (−24.3)
	longwave	0.46 (17.2)	0.34 (19.9)	0.20 (8.4)	0.22 (9.6)

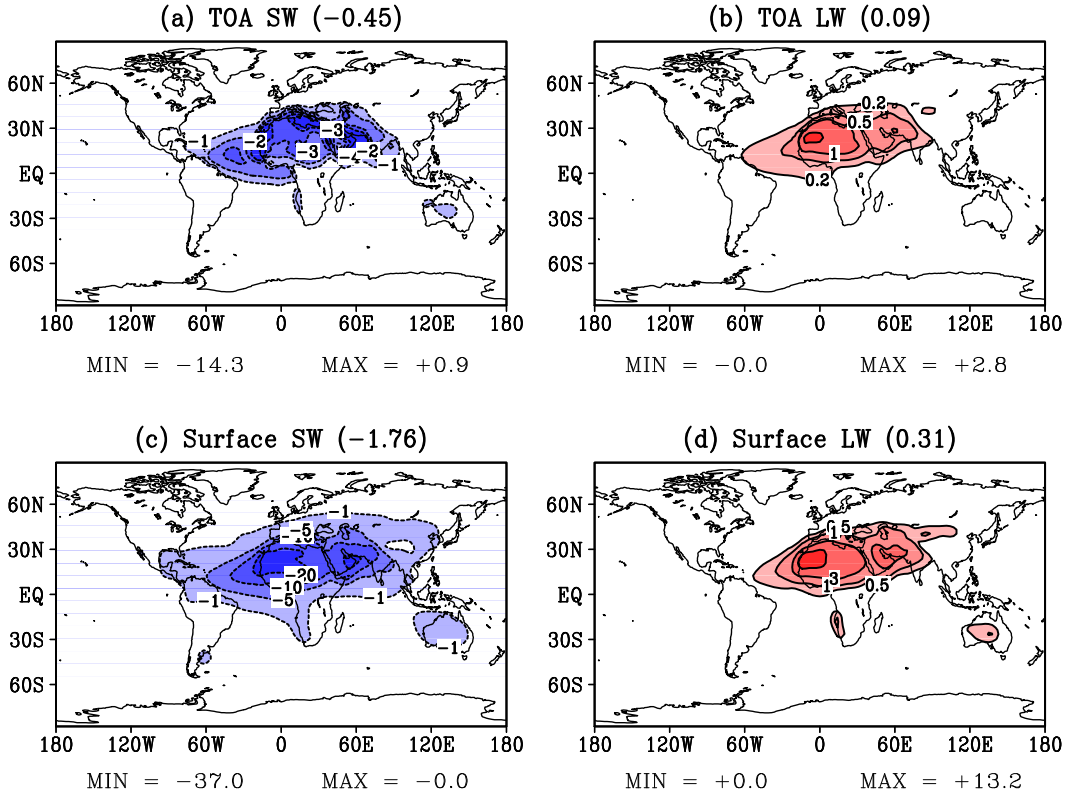

Fig. 5. Radiative forcing (RF) of dust aerosol in CAM3. (a) Shortwave RF at TOA; (b) longwave RF at TOA; (c) shortwave RF at surface; (d) longwave RF at surface. Positive values denote downward fluxes. The global averages are denoted in parentheses. Units: W m^{-2}.

and longwave RFs are generally stronger at the surface compared to that at the TOA.

3.4 *The climatic impact of dust aerosol*

Figure 8a shows the changes in the surface air temperature (TAS) in the presence of dust aerosol (FEDCTRL). Dust leads to a large decrease in TAS over the Sahara Desert and Arabian Peninsula. Such a reduction is attributed to the negative dust solar RF at the surface, which surpasses the warming by the thermal RF. However, the reductions in the surface temperature are not limited to dust source regions. Figure 8a shows a planetary teleconnection stretching from North Africa, across Eurasia, to North America. The surface cooling exists in northern and eastern Asia and over almost all of North America, while the surface warming is found in the Eastern Plains and at the northern edge of the Pacific Ocean. The dust-induced teleconnection pattern shown in Fig. 8a is quite similar to that reported by Kim et al. (2006) (cf. their Fig. 6a). Results indicate that dust RF leads to global responses by changing the regional atmospheric circulation.

On a global mean basis, dust leads to a surface cooling of 0.05 K. This reduction of TAS has a strong diurnal variation. Figures 8b and 8c show the dust-induced changes in daily maximum and minimum of TAS. The reductions in the averaged TAS are similar to those in the daily maximum TAS (TASMAX). TASMAX usually occurs in mid-late afternoon, while the daily minimum TAS (TASMIN) occurs after sunset. The attenuation of the solar energy by dust aerosol leads to a decrease in the daytime average TAS and in TASMAX as well. The net dust RF becomes positive at night because the solar RF is zero but the thermal component is still active. As a result, dust aerosol has a warming effect at midnight and TASMIN increases.

The reduction of TAS by dust has been reported in previous literature (e.g., Miller and Tegen, 1998; Shell and Somerville, 2007). Dust is predicted to lead to either a warming or a cooling at the surface depending on the characteristics of dust and the underlying surface conditions such as albedo and temperature (Tegen and Lacis, 1996; Liao and Seinfeld, 1998) and on the simulated relative importance of the solar and thermal effects of dust aerosol. For example, Weaver et al. (2002) obtained an increase of TAS in the presence of dust aerosol (cf. their Fig. 11b). In the CAM3, predicted dust particles are smaller compared with those in Tegen and Lacis (1996) and Weaver et al. (2002),

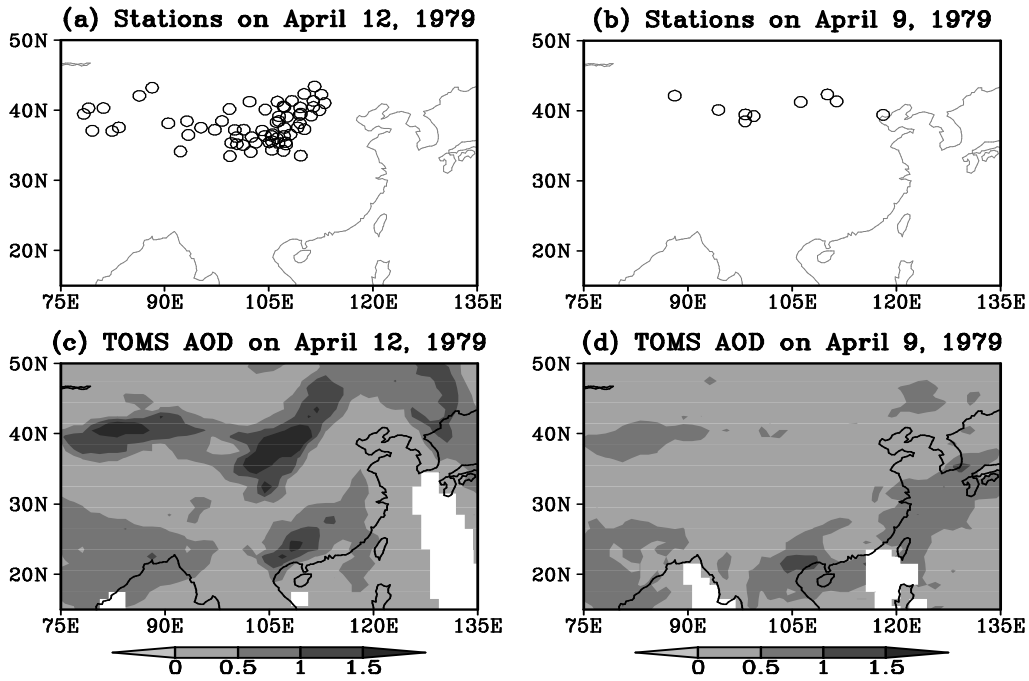

Fig. 6. Stations that reported "dust storm event" conditions on (a) 12 April 1979 and (b) 9 April 1979. The corresponding distributions of the TOMS AOD are shown in (c) and (d).

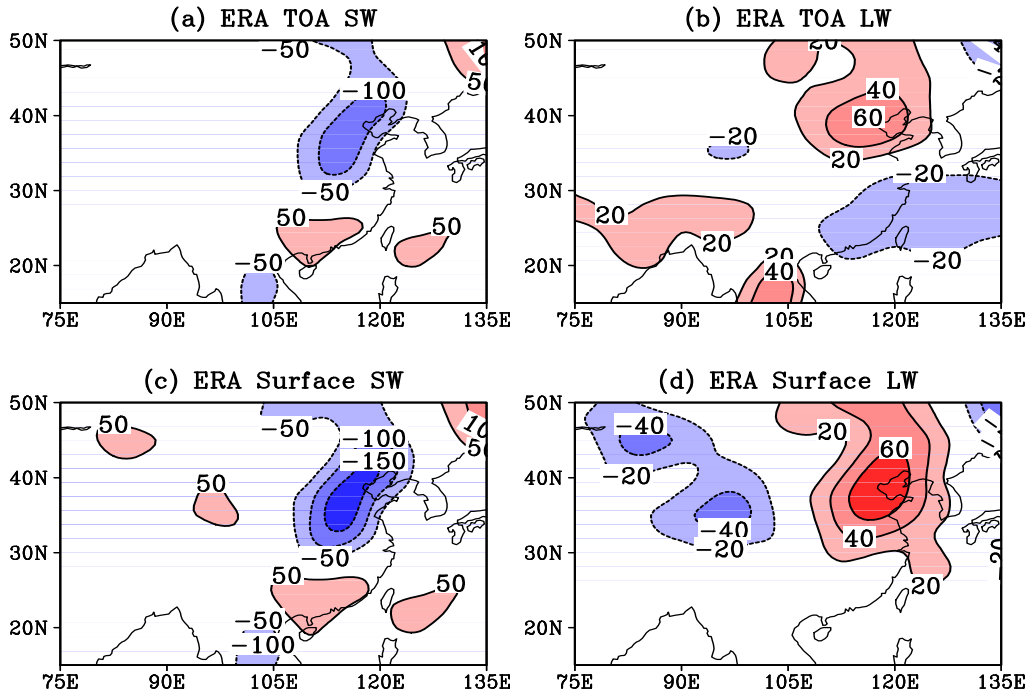

Fig. 7. Dust-induced changes in (a) shortwave radiation at the TOA; (b) longwave radiation at the TOA; (c) shortwave radiation at surface; (d) longwave radiation at surface during the severe dust storm period (12 April 1979), relative to a normal case (9 April 1979). Positive values denote downward fluxes. Units: W m^{-2}.

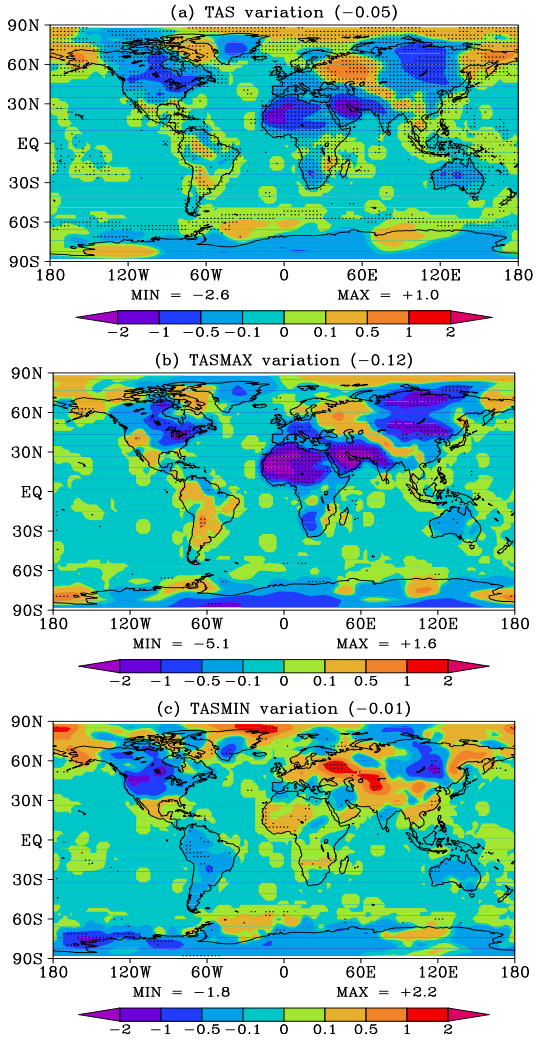

Fig. 8. Changes in (a) TAS; (b) daily maximum of TAS; (c) daily minimum of TAS in the presence of dust aerosol (FED-CTRL). Results that exceed the 0.005 significance level are denoted with dots. The global averages are denoted in parentheses. Units: K.

leading to a cooling effect by dust aerosol in the CAM3 which is stronger than that in other studies.

Although predicted changes in TAS differ in different models, the predicted dust-induced changes in air temperature at higher layers are generally consistent in different studies. Figure 9 shows the predicted changes in temperature at different vertical levels. The magnitudes of the changes in air temperature are smaller than that in the TAS. Over the Sahara Desert and Arabian Peninsula, reductions in temperature are predicted at 850 hPa (Fig. 9a) and increases are found above 500 hPa (Fig. 9b, 9c). The warming is caused by the absorption of solar energy by dust aerosol, (Alpert et al., 1998; Miller and Tegen, 1998; Weaver et al., 2002; Ramanathan and Ramana, 2005; Satheesh et al., 2007).

Together with the changes in temperature, other physical fields exhibit alterations (Fig. 10). The surface sensible heat flux shows a large reduction over the dust source regions (Fig. 10a). On a global average, the sensible heat flux is reduced by 0.53 W m^{-2}, resulting from the decreases in TAS shown in Fig. 8a. SST is kept constant in our simulations, leading to small changes in sensible heat flux between oceans and the atmosphere even after considering dust feedback. The latent heat flux also shows a global decrease (Fig. 10b). However, unlike the sensible heat fluxes, which are reduced mostly over the source regions, the reductions in the latent heat flux occur mostly over the

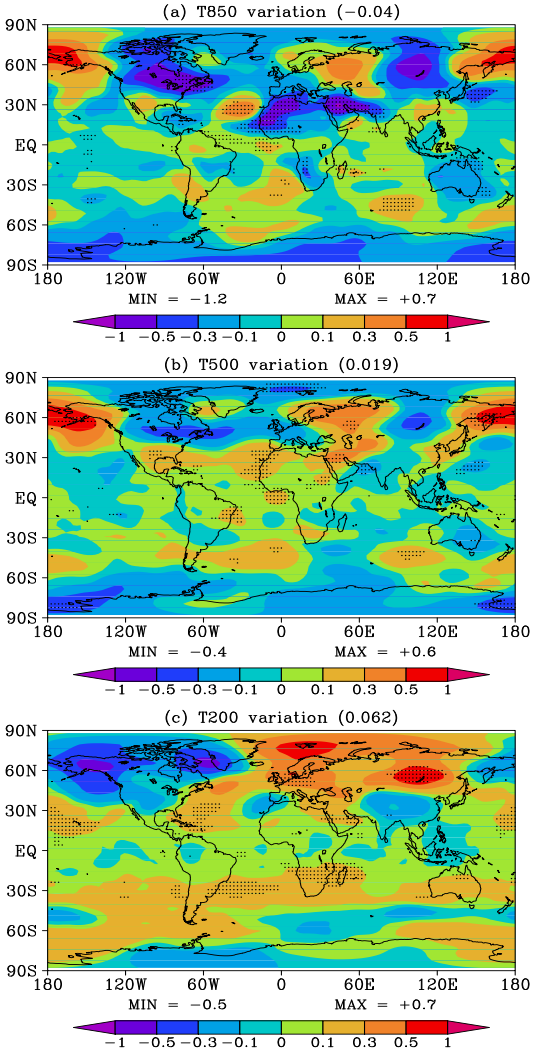

Fig. 9. Changes in air temperature at (a) 850 hPa; (b) 500 hPa; (c) 200 hPa in the presence of dust aerosol (FED-CTRL). Results that exceed the 95% confidence level are denoted with dots. The global averages are denoted in parentheses. Units: K.

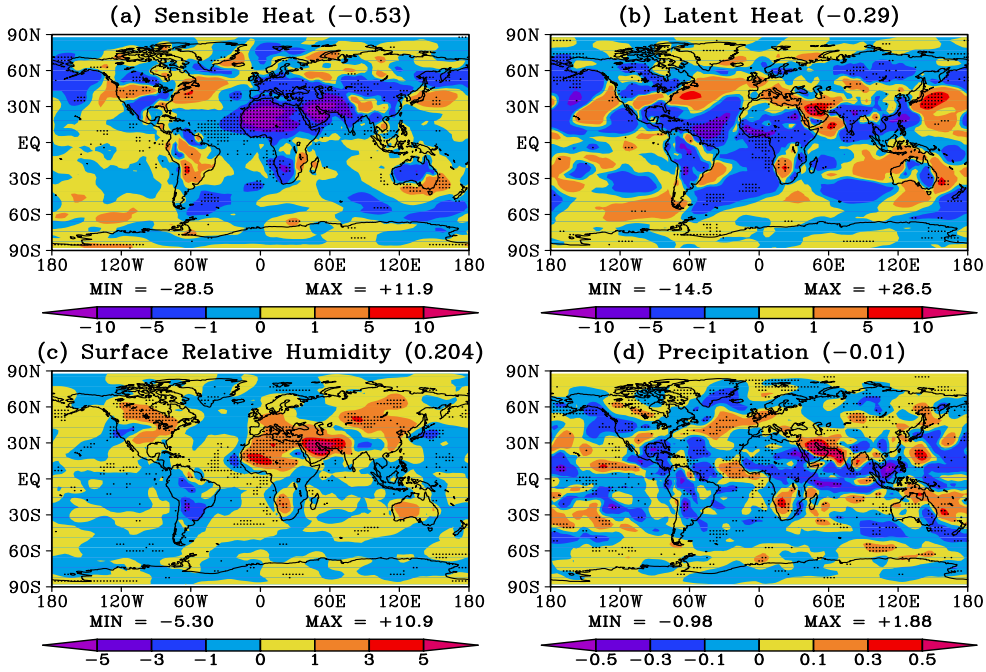

Fig. 10. Changes in meteorological fields in the presence of dust aerosol (FED-CTRL): (a) Sensible heat flux, units: W m^{-2}; (b) latent heat flux, units: W m^{-2}; (c) surface relative humidity, units: %; (d) precipitation, units: mm d^{-1}. Results that exceed the 95% confidence level are denoted with dots. The global averages are denoted in parentheses.

oceans. To compensate the surface radiation reductions caused by dust aerosol, the latent heat fluxes over the oceans are reduced (Miller and Tegen, 1998; Ramanathan and Ramana, 2005; Shell and Somerville, 2007).

Figure 10c shows the dust-induced changes in surface relative humidity (RHS). A widespread increase of RHS is predicted over North Africa and the Arabian Peninsula, which can be attributed to two factors. First, the increase in RHS corresponds to the increase in specific humidity over the same regions (not shown). Dust leads to surface cooling and a warming in the lower layers (1–3 km) (Fig. 8 and Fig. 9), increasing the stability of the atmosphere and hence reducing the vertical transport of moisture from the boundary layer (Ramanathan and Ramana, 2005). This effect surpasses the reduction in surface evaporation caused by the simulated reduction in surface temperature in the CAM3. Second, the saturated specific humidity decreases because of the reduction in TAS in the presence of dust aerosol. Consequently, the RHS show increases when considering the dust feedback.

Figure 10d shows the dust-induced changes in precipitation. Large areas of reductions in rainfall are predicted over dust sources and oceans, caused by the decreases in surface latent heat flux shown in Fig. 10b. On a global scale, dust leads to a reduction of 0.01 mm d^{-1} in precipitation, consistent with the results in Miller and Tegen (1998).

4. Summary and discussion

Direct climatic effects of dust aerosol are simulated with the CAM3 in this study. The GCM considers four dust size bins whose diameters range from 0.01 to 10 μm. The annual mean dust burden is 15.6 Tg, with the four dust bins accounting for 17%, 48%, 26%, and 9% of the burden, respectively. The seasonal variation of the DOT at 0.67 μm shows a maximum in the boreal summer (JJA) and a minimum in the boreal winter (DJF).

We updated the original radiative scheme in the CAM3 to consider the dust longwave effect. An exponential transmission approximation is used for mineral dust aerosol (Carlson and Benjamin, 1980), which considers the alterations in atmospheric transmissivity and emissivity by dust. With this implementation, we can calculate both the longwave and shortwave RFs of dust. The simulated shortwave RF is −0.45 W m^{-2} at the TOA and −1.76 W m^{-2} at the surface on a global average. Meanwhile, the longwave RF is +0.09 W m^{-2}at TOA and +0.31 W m^{-2} at surface. The net RF at TOA is −0.36 W m^{-2}, much smaller than the −1.45 W m^{-2} at the surface, indicating that dust aerosol causes an additional absorption of 1.1 W m^{-2} in the atmosphere.

The negative dust RF at the surface causes a cooling of about 0.5 K over the Sahara Desert and Arabian Peninsula. This reduction in TAS is mainly attributed to the decrease of TASMAX during the daytime. In the upper troposphere, the dust absorption induces a warming. The reduced surface temperature and the higher air temperature increase the atmospheric stability. Consequently, the upward transport of moisture is inhibited and the RHS shows increases. The sensible heat flux shows large reductions in dust source regions, which compensates the energy loss by the backscattering and absorption of dust. Since the SST is prescribed in this work, the latent heat fluxes over the oceans decrease so as to balance the reductions of surface radiation. As a result, precipitation decreases when considering the dust direct climatic effect.

Our model results show some common features when we compare them with previous studies. First, dust causes a global mean reduction of surface solar radiation of 1–2 W m^{-2} (Table 1), which is much larger than the -0.4 W m^{-2} by sulfate aerosol (Forster et al., 2007). Second, the solar RF at the TOA is much smaller than the forcing at the surface, which indicates the large absorption by dust aerosol (Miller and Tegen, 1998; Shi et al., 2008). Third, the thermal effect of dust is not negligible. The longwave effect of dust can partly offset the shortwave effect, which leads to a small net climatic effect of dust (Reddy et al., 2005b; Christopher and Jones, 2007). Fourth, dust aerosol leads to warming at the higher levels, as reported by many studies (e.g., Alpert et al., 1998; Ramanathan and Ramana, 2005). Finally, the decrease in radiation at the surface is partly balanced by a reduction in sensible heat flux and latent heat flux at the surface (Miller and Tegen, 1998; Shell and Somerville, 2007).

Different studies show uncertainties in simulating dust-induced changes in surface temperature. Dust solar RF cools the surface during daytime, but the thermal RF warms the surface at midnight. These two opposite effects counteract each other and lead to different net changes in temperature in different models. Some studies have obtained cooling at the surface in the presence of dust (Miller and Tegen, 1998; Shell and Somerville, 2007). Other studies found that dust leads to warming throughout the whole troposphere (Weaver et al., 2002). To reduce model uncertainties, more observations are required to accurately represent the size distribution, optical parameters, and vertical distribution of dust particles, the key factors that influence the radiative characteristics of dust aerosol (Tegen and Lacis, 1996; Liao and Seinfeld, 1998; Claquin et al., 1998).

There are also uncertainties in the simulated regional and global responses to dust radiative forcing. The propagation of dust-induced perturbations through large scale teleconnections as simulated in our study agrees with the results reported by Kim et al. (2006). This finding enriches our scope in understanding the role of dust aerosol. However, more observations and simulations are needed to consolidate this conclusion.

The simulation of the dust direct climatic effect in this study can be further improved. The offline dust model underestimates dust concentrations in Central Asia, which may lead to an underestimate of climate responses to the dust radiative effect over Asia. The importance of Asian dust was recently reported by Huang et al. (2009), who found large atmospheric heating by dust aerosol during a dust event over the Taklimakan region by combining Cloud-Aerosol Lidar and Infrared Pathfinder Satellite Observations (CALIPSO) measurements and a Fu-Liou radiation model. In addition, the dust cycle should be two-way coupled with climate. While dust influences climate, climate change can alter dust climatology in turn. For example, the reductions in surface wind speed and the increases in RHS can inhibit dust emissions (Miller et al., 2004b), and the decreases in rainfall will reduce the rainout of dust, increasing the lifetime of dust in the atmosphere (Ramanathan and Ramana, 2005). Such feedbacks will be reported subsequently in our future studies.

Acknowledgements. We are grateful to Prof. ZHOU Tianjun and Dr. WEN Xinyu for their guidance concerning the CAM3 model. Prof. Charlie Zender from the University of California at Irvine provided helpful suggestions about dust longwave simulation. This research was supported by the Key Project of Chinese Academy of Sciences under Grant KZCX2-YW-Q11-03, and was jointly supported by the National Basic Research Program of China ("973" program) under Grant 2006CB403705, by the Key Project of Chinese Academy of Sciences under Grants KZCX2-YW-Q1-02, KZCX2-YW-205, and KZCX2-YW-219, and by the National Natural Science Foundation of China under Grant No. 40631005.

REFERENCES

Ackerman, S. A., and H. Chung, 1992: Radiative effects of airborne dust on regional energy budgets at the top of the atmosphere. *J. Appl. Meteor.*, **31,** 223–233.

Alpert, P., Y. J. Kaufman, Y. Shay-El, D. Tanre, A. d. Silva, S. Schubert, and J. H. Joseph, 1998: Quantification of dust-forced heating of the lower troposphere. *Nature*, **395,** 367–370.

Carlson, T. N., and S. G. Benjamin, 1980: Radiative heating rates for Saharan dust. *J. Atmos. Sci.*, **37,** 193–213.

Cautenet, G., M. Legrand, S. Cautenet, B. Bonnel, and G. Brogniez, 1991: Thermal impact of Saharan dust over land. Part I: Simulation. *J. Appl. Meteor.*, **31,** 166–180.

Christopher, S. A., and T. Jones, 2007: Satellite-based assessment of cloud-free net radiative effect of dust aerosols over the Atlantic Ocean. *Geophys. Res. Lett.*, **34,** L02810, doi: 02810.01029/02006GL027783.

Claquin, T., M. Schulz, Y. Balkanski, and O. Boucher, 1998: Uncertainties in assessing radiative forcing by mineral dust. *Tellus* (*B*), **50,** 491–505.

Collins, W. D., P. J. Rasch, B. E. Eaton, B. V. Khattatov, J. F. Lamarque, and C. S. Zender, 2001: Simulating aerosols using a chemical transport model with assimilation of satellite aerosol retrievals: Methodology for INDOEX. *J. Geophys. Res.*, **106,** 7313–7336.

Collins, W. D., and Coauthors, 2004: Description of the NCAR Community Atmosphere Model (CAM 3.0). NCAR Technical Note NCAR/TN-464+STR, NCAR, Boulder, CO, 226pp.

Dufresne, J.-L., C. Gautier, P. Ricchiazzi, and Y. Fouquart, 2002: Longwave scattering effects of mineral aerosols. *J. Atmos. Sci.*, **59,** 1959–1966.

Forster, P., and Coauthors, 2007: Changes in Atmospheric Constituents and in Radiative Forcing. *Climate Change 2007: The Physical Science Basis. Contribution of Working Group I to the Fourth Assessment Report of the Intergovernmental Panel on Climate Change*, Cambridge University Press, 131–217.

Ginoux, P., M. Chin, I. Tegen, J. M. Prospero, B. Holben, O. Dubovik, and S.-J. Lin, 2001: Sources and distributions of dust aerosols simulated with the GOCART model. *J. Geophys. Res.*, **106,** 20255–20273.

Haywood, J., and Coauthors, 2003: Radiative properties and direct radiative effect of Saharan dust measured by the C-130 aircraft during SHADE: 1. Solar spectrum. *J. Geophys. Res.*, **108,** 8577, doi: 8510.1029/2002JD002687.

Huang, J., and Coauthors, 2009: Taklimakan dust aerosol radiative heating derived from CALIPSO observations using the Fu-Liou radiation model with CERES constraints. *Atmospheric Chemistry and Physics Discussion*, **9**, 5967–6001.

Jacobson, M. Z., 2001: Global direct radiative forcing due to multicomponent anthropogenic and natural aerosols. *J. Geophys. Res.*, **106,** 1551–1568.

Kaufman, Y. J., D. Tanré, O. Dubovik, A. Karnieli, and L. A. Remer, 2001: Absorption of sunlight by dust as inferred from satellite and ground-based remote sensing. *Geophys. Res. Lett.*, **28,** 1479–1482.

Kim, M. K., W. K. M. Lau, M. Chin, K. M. Kim, Y. C. Sud, and G. K. Walker, 2006: Atmospheric teleconnection over Eurasia induced by aerosol radiative forcing during boreal spring. *J. Climate*, **19,** 4700–4718.

Liao, H., and J. H. Seinfeld, 1998: Radiative forcing by mineral dust aerosols: Sensitivity to key variables. *J. Geophys. Res.*, **103,** 31637–31645.

Liao, H., J. H. Seinfeld, P. J. Adams, and L. J. Mickley, 2004: Global radiative forcing of coupled tropospheric ozone and aerosols in a unified general circulation model. *J. Geophys. Res.*, **109,** D16207, doi: 16210.11029/12003JD004456.

Liu, W., Q. Feng, T. Wang, Y. W. Zhang, and J. H. Shi, 2004: Physicochemistry and mineralogy of storm dust and dust sediment in northern China. *Adv. Atmos. Sci.*, **21,** 775–783.

Markowicz, K. M., P. J. Flatau, A. M. Vogelmann, P. K. Quinn, and E. J. Welton, 2003: Clear-sky infrared aerosol radiative forcing at the surface and the top of the atmosphere. *Quart. J. Roy. Meteor. Soc.*, **129,** 2927–2947.

Miller, R. L., and I. Tegen, 1998: Climate response to soil dust aerosols. *J. Climate*, **11,** 3247–3267.

Miller, R. L., I. Tegen, and J. Perlwitz, 2004a: Surface radiative forcing by soil dust aerosols and the hydrologic cycle. *J. Geophys. Res.*, **109,** D04203, doi: 04210.01029/02003JD004085.

Miller, R. L., J. Perlwitz, and I. Tegen, 2004b: Feedback upon dust emission by dust radiative forcing through the planetary boundary layer. *J. Geophys. Res.*, **109,** D24209, doi: 24210.21029/22004JD004912.

Myhre, G., and F. Stordal, 2001: Global sensitivity experiments of the radiative forcing due to mineral aerosols. *J. Geophys. Res.*, **106,** 18193–18204.

Penner, J. E., and Coauthors, 2001: Aerosols : Their direct and indirect effects. *Climate Change 2001 : The Scientific Basis, Contribution of Working Group I to the Third Assessment Report of the Intergovernmental Panel on Climate Change*, Cambridge University Press, 291–336.

Perlwitz, J., I. Tegen, and R. L. Miller, 2001: Interactive soil dust aerosol model in the GISS GCM: 1. Sensitivity of the soil dust cycle to radiative properties of soil dust aerosols. *J. Geophys. Res.*, **106,** 18167–18192.

Prospero, J. M., P. Ginoux, O. Torres, S. E. Nicholson, and T. E. Gill, 2002: Environmental characterization of global sources of atmospheric soil dust identified with the nimbus 7 total ozone mapping spectrometer (TOMS) absorbing aerosol product. *Rev. Geophys.*, **40,** 1002, doi: 1010.1029/2000RG000095.

Ramanathan, V., and M. V. Ramana, 2005: Persistent, widespread, and strongly absorbing haze over the Himalayan foothills and the Indo-Gangetic Plains. *Pure Appl. Geophys.*, **162,** 1609–1626.

Rasch, P. J., N. M. Mahowald, and B. E. Eaton, 1997: Representations of transport, convection, and the hydrologic cycle in chemical transport models: Implications for the modeling of short-lived and soluble species. *J. Geophys. Res.*, **102,** 28127–28138.

Reddy, M. S., O. Boucher, N. Bellouin, M. Schulz, Y. Balkanski, J. L. Dufresne, and M. Pham, 2005a: Estimates of global multicomponent aerosol optical depth and direct radiative perturbation in the Laboratoire de Meteorologie Dynamique general circulation model. *J. Geophys. Res.*, **110,** D10S16, doi: 10.1029/2004JD004757.

Reddy, M. S., O. Boucher, Y. Balkanski, and M. Schulz, 2005b: Aerosol optical depths and direct radiative perturbations by species and source type. *Geophys. Res. Lett.*, **32,** L12803, doi: 12810.11029/12004GL021743.

Sassen, K., 2002: Indirect climate forcing over the western US from Asian dust storms. *Geophys. Res. Lett.*, **29,** 1465, doi: 1410.1029/2001GL014051.

Satheesh, S. K., C. B. S. Dutt, J. Srinivasan, and U. R. Rao, 2007: Atmospheric warming due to dust absorption over Afro-Asian regions. *Geophys. Res. Lett.*, **34,** L04805, doi: 04810.01029/02006GL028623.

Shell, K. M., and R. C. J. Somerville, 2007: Direct radiative effect of mineral dust and volcanic aerosols in a simple aerosol climate model. *J. Geophys. Res.*, **112,** D03206, doi: 03210.01029/02006JD007198.

Shi, G., H. Wang, B. Wang, W. Li, S. Gong, and T. Zhao, 2005: Sensitivity experiments on the effects of optical properties of dust aerosols on their radiative forcing under clear sky condition. *J. Meteor. Soci. Japan*, **83A,** 333–346.

Shi, G., B. Wang, H. Zhang, J. Zhao, S. Tan, and T. Wen, 2008: The radiative and climatic effects of atmospheric aerosols. *Chinese J. Atmos. Sci.*, **32,** 826–840. (in Chinese)

Sokolik, I. N., and O. B. Toon, 1996: Direct radiative forcing by anthropogenic airborne mineral aerosols. *Nature*, **381,** 681–683.

Sokolik, I. N., and O. B. Toon, 1999: Incorporation of mineralogical composition into models of the radiative properties of mineral aerosol from UV to IR wavelengths. *J. Geophys. Res.*, **104,** 9423–9444.

Tanaka, T. Y., T. Aoki, H. Takahashi, K. Shibata, A. Uchiyama, and M. Mikami, 2007: Study of the sensitivity of optical properties of mineral dust to the direct aerosol radiative perturbation using a global aerosol transport model. *SOLA*, **3,** 33–36.

Tegen, I., and A. A. Lacis, 1996: Modeling of particle size distribution and its influence on the radiative properties of mineral dust aerosol. *J. Geophys. Res.*, **101,** 19237–19244.

Tegen, I., P. Hollrig, M. Chin, I. Fung, D. Jacob, and J. Penner, 1997: Contribution of different aerosol species to the global aerosol extinction optical thickness: Estimates from model results. *J. Geophys. Res.*, **102,** 23895–23916.

Torres, O., P. K. Bhartia, J. R. Herman, A. Sinyuk, and B. Holben, 2002: A long term record of aerosol optical thickness from TOMS observations and comparison to AERONET measurements. *J. Atmos. Sci.*, **59,** 398–413.

Wang, Z., H. Ueda, and M. Huang, 2000: A deflation module for use in modeling long-range transport of yellow sand over East Asia. *J. Geophys. Res.*, **105,** 26947–26959.

Weaver, C. J., P. Ginoux, N. C. Hsu, M.-D. Chou, and J. Joiner, 2002: Radiative Forcing of Saharan Dust: GOCART Model Simulations Compared with ERBE Data. *J. Atmos. Sci.*, **59,** 736–747.

Woodward, S., 2001: Modeling the atmospheric life cycle and radiative impact of mineral dust in the Hadley Centre climate model. *J. Geophys. Res.*, **106,** 18155–18166.

Wu, J., C. B. Fu, W. M. Jiang, H. N. Liu, and R. H. Zhao, 2005: A preliminary simulation study of direct radiative forcing of mineral dust aerosol over the East Asia region. *Chinese J. Geophys.*, **48,** 1250–1260. (in Chinese)

Xie, J. X., and X. A. Xia, 2008: Long-term trend in aerosol optical depth from 1980 to 2001 in north China. *Particuology*, **6,** 106–111.

Yoshioka, M., N. M. Mahowald, A. J. Conley, W. D. Collins, D. W. Fillmore, C. S. Zender, and D. B. Coleman, 2007: Impact of desert dust radiative forcing on Sahel precipitation: Relative importance of dust compared to sea surface temperature variations, vegetation changes, and greenhouse gas warming. *J. Climate*, **20,** 1445–1467.

Yue, X., H. Wang, Z. Wang, and K. Fan, 2009: Simulation of dust aerosol radiative feedback using the Global Transport Model of Dust: 1. Dust cycle and validation. *J. Geophys. Res.*, **114,** D10202, doi: 10210.11029/12008JD010995.

Zender, C. S., H. Bian, and D. Newman, 2003: Mineral Dust Entrainment and Deposition (DEAD) model: Description and 1990s dust climatology. *J. Geophys. Res.*, **108,** 4416, doi: 4410.1029/2002JD002775.

Zhang, H. M., and M. F. Modest, 2002: Evaluation of the Planck-mean absorption coefficients from HITRAN and HITEMP databases. *Journal of Quantitative Spectroscopy and Radiative Transfer*, **73,** 649–653.

Zhou, Z., X. Wang, and R. Niu, 2002: Climate characteristics of sandstorm in China in recent 47 years. *Journal of Applied Meteorological Science*, **13,** 193–200. (in Chinese)

Zhou, Z. J., and G. C. Zhang, 2003: Typical severe dust storms in northern China during 1954–2002. *Chinese Science Bulletin*, **48,** 2366–2370.